Assessment of Transition Modeling Capability in OVERFLOW with Emphasis on Swept-Wing Configurations

Balaji Shankar Venkatachari,[*] Pedro Paredes[†]
National Institute of Aerospace, Hampton, VA 23666

Joseph M. Derlaga,[‡] Pieter Buning,[§] Meelan Choudhari,[**] Fei Li,[††] and Chau-Lyan Chang[‡‡]
NASA Langley Research Center, Hampton, VA 23681

In preparation for comparisons with data obtained from the recently concluded experiments in the National Transonic Facility at the NASA Langley Research Center on the new common research model with natural laminar flow (CRM-NLF), an assessment of the current transition modeling capability in the NASA OVERFLOW 2.2o code has been carried out. A combination of the available experimental data and linear stability analysis is used to evaluate the accuracy and robustness of these models for selected swept-wing type configurations, with significant crossflow. An additional goal for this work involves providing a comparative assessment of the relevant transition models in the context of a single flow solver and identifying model limitations as well as the potential for future improvements that would help strengthen the physical basis of such transition models. Included in this investigation is an assessment of the sensitivities of the underlying transition models to grid resolution (wall-normal, as well as streamwise and spanwise) and the values of extra input parameters such as the level of surface roughness and freestream turbulence variables. The flow configurations targeted in this assessment include the NASA NLF(2)-0415 swept-wing configuration, the sickle-shaped wing introduced by the Technical University of Braunschweig, and the wing-body configuration of the CRM model from the fourth and fifth AIAA CFD Drag Prediction Workshops.

Nomenclature

C_f = skin friction coefficient [nondimensional]
C_p = surface pressure coefficient [nondimensional]
K = surface roughness height (rms) [μm]
Re_c = Reynolds number based on freestream variables and chord or mean aerodynamic chord [nondimensional]
$Re_{\theta t}$ = transition onset momentum thickness Reynolds number based on freestream conditions [nondimensional]
U = local freestream velocity [m/s]
x/c = chordwise coordinate scaled by reference chord length [nondimensional]
y^+ = near wall grid spacing in wall units [nondimensional]
α = angle of attack [deg]
η = semispan location nondimensionalized by semispan length [nondimensional]
μ = dynamic viscosity [kg/(m.s)]
ρ = density [kg/m^3]
θ = momentum thickness [mm]

---

[*] Sr. Research Engineer, Senior member, AIAA
[†] Research Engineer, Senior Member, AIAA
[‡] Research Scientist, Computational AeroSciences Branch, Member, AIAA
[§] Aerospace Technologist, Computational AeroSciences Branch, Associate Fellow, AIAA
[**] Aerospace Technologist, Computational AeroSciences Branch, Fellow, AIAA
[††] Aerospace Technologist, Computational AeroSciences Branch
[‡‡] Aerospace Technologist, Computational AeroSciences Branch, Associate Fellow, AIAA

I. Introduction

According to CFD Vision 2030 [1], the most critical area in computational fluid dynamics (CFD) simulation capability that will remain a pacing item for the foreseeable future is the ability to adequately predict viscous flows with boundary layer transition from laminar to turbulent and flow separation. A majority of CFD computations are carried out under the assumption that the boundary layer is turbulent everywhere, and they often use the computationally efficient Reynolds-averaged Navier-Stokes (RANS) models. However, for certain applications such as wings designed with natural laminar flow (NLF) or unmanned aerial vehicle designs, such strong assumptions can lead to significant errors in performance estimation. Furthermore, most of the RANS models are incapable of modeling the process of boundary layer transition from laminar-to-turbulent flow because of the complexity involved in the physics of the transition onset process, and the inherent averaging process in the RANS procedure makes it difficult to capture the development of the linear disturbances and subsequent nonlinear growth and eventual breakdown.

Direct numerical simulations (DNS) and wall-resolved large-eddy simulations (WRLES) are capable of simulating the complete physical process of the onset of boundary layer transition and the breakdown of laminar into turbulent flow. However, even with the current state-of-the-art tools in high performance computing, these approaches are too expensive to permit the analysis of realistic configurations at high Reynolds numbers due to the extreme requirements of spatio-temporal resolutions. Moreover, DNS and WRLES require accurate specification of the initial and boundary conditions to account for a correct representation of the factors that excite the instabilities in the flow, and this information is often not fully available from most wind-tunnel and flight tests.

Using semiempirical correlations based on linear stability theory (LST), such as the e^N method introduced by Smith and Gamberoni [2] and van Ingen [3], remains one of the most widely used approaches for the prediction of transition onset locations in aircraft design computations. The LST equations are derived from the linearized Navier-Stokes equations to track the evolution of small amplitude, fixed frequency disturbances under the parallel flow assumption. The e^N method does require the specification of a critical N-factor that must be obtained from correlations against experimentally measured transition locations. Transition analysis using the parabolized stability equations (PSE) [4] has less-restrictive assumptions and can more easily account for the effects of a nonparallel basic state, curvatures in geometry, and nonlinear modal interactions of the laminar instabilities. Both LST and PSE can account for the amplification of the dominant primary instabilities encountered on aircraft wings, namely, the Tollmien-Schlichting waves and the stationary/travelling crossflow vortices. However, the application of these approaches toward a coupled computation of laminar, transitional, and fully turbulent parts of a boundary layer entails an increased computational cost as well as complexity; it also suffers from a lack of robustness and often requires adequate understanding of transition physics and hydrodynamic stability theory that typical users of CFD codes may not have. To alleviate or circumvent these shortcomings, surrogate models are often used in lieu of the direct computation of stability characteristics based on the laminar boundary layer information provided by the flow solver. There are a number of successful implementations of CFD codes that combine stability-based transition predictions with RANS-based turbulence modeling, for instance see Refs. [5–12]. However, such models usually suffer from the need to have sufficiently well resolved boundary layer profiles in the laminar baseflow computations, including the wall-normal derivatives of velocities and temperature, or at least, the need to compute integral boundary layer parameters that may be used as a proxy to the laminar profiles themselves. These restrictions are difficult to overcome in modern CFD codes that rely upon massive parallelization and the use of unstructured grids [13].

Given that the vehicle performance is often characterized in terms of integral quantities such as load/moment coefficients or through pressure/skin-friction distribution, capturing the detailed physics of the transition to turbulence in itself is less important than the overall impact of the transition on the development of the boundary layer and its impact on the aforementioned quantities. Due to the previously mentioned reasons associated with robustness and user expertise as well as the general requirement of reducing the computational cost requirements associated with transition prediction, the efforts to develop transition models that represent the most critical components of the underlying physics and can be embedded into a RANS framework have gained substantial ground [14–23]. For reasons of computational efficiency, these

models often require that only local information be used to model transition, instead of using detailed boundary layer profiles for stability analysis or even integral-boundary layer parameters that may be used in metamodels for the stability characteristics. The RANS-based transition models often rely on solving additional transport equations and using correlations that determine the onset of transition, allowing the codes to switch between operating in the laminar and turbulent modes. This approach clearly overcomes some of the aforementioned limitations of stability-based transition prediction and is well-suited for generalizing the established process for turbulent flow computations in a cost effective manner. However, by virtue of lacking an adequate representation of the complex transition process, such models are also less amenable to an extrapolation to new configurations and must be validated on a case by case basis in general. More details on the various approaches currently being used to predict/model transition can be found in Refs. [24, 25].

The present research seeks to blend the so-called physics-based approach for transition modeling with the RANS-based approaches, with the eventual goal of developing a reliable and cost efficient, yet robust and user-friendly approach for integrated modeling of laminar-turbulent transition. As an initial step toward that goal, the present paper is focused on a detailed assessment of the existing RANS-based approach to modeling transition in the context of selected canonical flow configurations, with an emphasis on swept-wing configurations (where the RANS-based models have received less scrutiny) and a single flow solver, namely, the OVERFLOW solver [26] developed by NASA.

NASA recently completed a series of experiments in the National Transonic Facility that focused on the new common research model with natural laminar flow (CRM-NLF) [27–29]. In a typical transport aircraft wing with high sweep, transition occurs as a result of crossflow (CF) instability and/or Tollmien-Schlichting (TS) instability, provided that the attachment line remains laminar. The CRM-NLF wing has been designed to modify the surface pressure distribution in such a way that the overall amplification of both of these instabilities is reduced. CF growth is attenuated through a rapid acceleration near the leading edge (achieved via a sufficiently smaller leading edge radius), while the amplification of TS waves is controlled by creating a slightly favorable pressure gradient. The NLF design also addresses attachment line contamination and transition due to attachment line instabilities. The earlier RANS-based transition models were designed to account for transition caused by either TS waves, or some form of bypass transition, or as a result of flow separation; however, they did not account for crossflow effects very well. In the last few years, however, there has been an increased interest in incorporating the crossflow effects within the transition models [30–36]. Hence, as the precursor to a detailed comparison of the data obtained from the NASA CRM-NLF experiments, this paper seeks to assess the performance of some of the transition models available within the NASA OVERFLOW 2.2o code [26], specifically in regard to computing the flow over swept-wing configurations where one or both of the TS and crossflow instabilities may dominate the transition process, depending on the details of the surface pressure distribution and the flow Reynolds number. The models will be evaluated for their accuracy and robustness by using a combination of experimental data and linear stability analyses, with the intention of identifying model deficiencies and developing potential solutions to address them. The configurations tested include the NASA NLF(2)-0415 swept-wing configuration [37–39], the sickle-shaped wing introduced by the Technical University of Braunschweig [40], and the wing-body configuration of the CRM model from AIAA CFD Drag Prediction workshops IV and V [41]. The paper is organized as follows. Section II presents a brief overview of the OVERFLOW solver and the transition models evaluated in the study. The results from the evaluation of the transition models for the chosen suite of three test cases is discussed in Section III. Subsection III.A also contains details about recalibration of one the transition models used as part of the work. The conclusions are presented in the last section.

II. Flow Solver and Transition Models

The NASA OVERFLOW 2.2o [26] is an implicit structured overset grid Navier-Stokes solver that is capable of computing time-accurate and steady-state solutions via several options for spatial and temporal discretization. RANS-based transition models available in OVERFLOW 2.2o include: (i) the two-equation Langtry-Menter transition model (LM2009) [18] based on the year 2003 version of Menter's shear-stress transport (SST) RANS model [42], along with the modifications proposed by Langtry et al. [32] to account for crossflow induced transition (LM2015); (ii) Coder's [22, 23] 2017b version of the amplification factor transport (AFT2017b) equation-based model that uses the Spalart-Allmaras (SA) model [43]; and (iii) the Medida-Baeder transition model [19], which is a reformulation of the Langtry-Menter transition model to allow for integration with the SA model. There have been additional proposed modifications to the Medida-Baeder model that account for the effects of crossflow instability [30], but those have not yet been

implemented into OVERFLOW. The correlation-based-transition models by Langtry and Menter solve two equations, with one transport equation for the local transition onset momentum thickness Reynolds number ($\widetilde{Re_{\theta t}}$) and another one for transport of intermittency. The AFT2017b model also solves two equations: one for the transport of the amplification factor and another one for the transport of intermittency. Hence, from the perspective of the computational cost, the AFT2017b and Medida-Baeder models require slightly less work in comparison to the LM2009/LM2015 models due to the framework of SA turbulence model used in the implementation of the former two models. One aspect of note is that the OVERFLOW 2.2o implementation of the Langtry-Menter transition model is based upon the two-equation SST 2003 turbulence model [42], similar to the original formulation of the transition model [17]. However, most of the recent literature [18, 31, 33] that describes the Langtry-Menter model, as well as the subsequent improvements to handle crossflow effects, references Menter's original (i.e., standard) SST model [44]. Hence, the model coefficients that characterize the modifications to account for crossflow transition need to be recalibrated for the implementation based on the SST-2003 RANS model.

III.Test Cases and Results

All of the results reported in this section were obtained by running the flow solver in a steady-state manner by using the 3rd-order Roe upwind scheme [45] and the unfactored successive symmetric overrelaxation (SSOR) implicit solution algorithm [46]. The set of results presented herein are based on (i) the AFT 2017b transition model, (ii) the LM2009 model, and (iii) the LM2015 model that accounts for crossflow induced transition. As the Medida-Baeder model [19] is a variant of the Langtry-Menter transition model, it is not unreasonable to expect that any inference drawn about the performance of the Langtry-Menter transition model will carry over to the Medida-Baeder model as well, but that will be verified once the crossflow modifications for the Medida-Baeder model have been implemented in OVERFLOW.

A. NLF(2)-0415 45º Swept Wing

The data from the experiments on the swept wing configuration of the NLF(2)-0415 airfoil [47] carried out by Dagenhart et al. [37] and Radeztsky et al. [38] in the low-turbulence unsteady wind tunnel facility at the Arizona State University, forms the crux of both formulating and calibrating the LM2015 transition model to predict the transition scenarios dominated by stationary crossflow (SCF) instability. Although there have been other attempts at including crossflow effects into the LM2009 model [33–35], most of them do not account for the surface roughness, which is one of the most critical aspects in determining the onset of crossflow induced transition. The above-mentioned experiments provided measurements that characterize the dependence of the transition location on the flow Reynolds number and a scalar measure of the roughness height distribution, enabling Langtry et al. [32] to create a correlation based on that data, similar to the approach originally pursued by Crouch and Ng [48]. Given the importance of this experiment to the LM2015 model, we describe it here in detail, so that the CFD computations can be performed in a manner that closely resembles the experiment.

The 45º swept wing based on the NLF(2)-0415 airfoil was placed vertically in the wind-tunnel and was mounted on an axis running through the quarter chord and parallel to the wing leading edge. The wing had a streamwise chord of 1.83 m (unswept chord of 1.294m). The wind-tunnel cross section was 1.37 m by 1.37 m. The mounting axis was slightly off-center within the test section as indicated in Fig. 1, such that the top surface of the airfoil was closer to the front wall of the wind tunnel, as indicated in Fig. 1, in comparison to the back wall. The wing was operated at an angle of attack of -4º, to achieve a long extent of favorable pressure gradient on the upper surface of the wing, so that TS waves are stabilized and cross flow vortices get amplified. Contoured end liners were used to simulate infinite swept-wing flow. The freestream turbulence in the tunnel, in the model installed configuration, was estimated to be around 0.09% [39]. Transition measurements on the upper surface of the wing were made via flow visualizing studies based on naphthalene sublimation and liquid crystal coating over the wing surface. Detailed streamwise velocity measurements were made with hot wire anemometers at several locations. In the experiments by Dagenhart et al. [37], the model had a painted surface with an rms roughness value of 3.3 μm (peak to peak 9 μm). In the additional experiments carried out by Radeztsky et al. [38], the rms surface roughness levels were significantly lower at k = 0.5 μm and 0.25 μm, respectively. Additional details on the experiment can be found in Ref. [39].

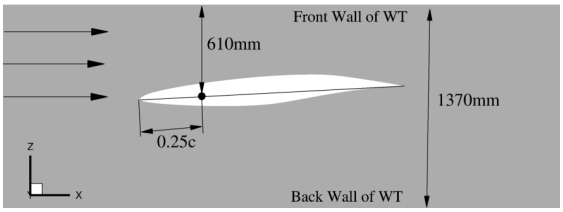

Fig. 1. Schematic of the wind tunnel installation, as seen from the bottom of the wind tunnel.

The CFD computations were predominantly performed using a baseline grid that had a "C-grid" topology around the airfoil, created using the Chimera grid tool (CGT) [49]. The wing had 601 points in the chord wise direction (301 on each side of the wing, with a leading edge spacing of 0.02% relative to the chord length and a trailing edge spacing of 0.1% chord). The wall normal spacing was $y^+ = 0.125$ based on the conditions at 10% chord and the geometric stretching factor in the wall normal direction was approximately 1.05. To mimic the infinite swept configuration, the spanwise length was set at two chords, with 3 points across the span and the 2D boundary condition was enforced at one of the end planes. Given the large size of the wing relative to the tunnel cross section, substantial blocking effects were both expected and observed during the experiments. As a result, two configurations were created for the CFD computations: (i) the free-air configuration that had just a single block grid around the airfoil and extended about 50 chord distances outward; and (ii) a wind tunnel installed configuration that included the tunnel walls in the direction above and below the surfaces of the wing as indicated in Fig. 1. For the wind tunnel configuration, an additional Cartesian grid was created for the wind tunnel without the wing model and assembled using PEGASUS5 [50]. The wind tunnel walls were specified as inviscid boundaries. Depending on the configuration, the total number of wall normal grid points for the near body grid varied from 451 in the case of free-air to 251 in the case of the installed configuration.

The computed surface pressure distributions, for both the free-air and the installed configurations are shown in Fig. 2(a), along with its comparison with the predictions based on simpler airfoil codes (Eppler and MCARF) as given by Dagenhart and Saric in Figs. 42 and 43 of Ref. [39]. The figure shows considerable differences between the pressure distributions for the free-air and installed configurations. The upper wing surface has a stronger favorable pressure gradient in the case of the installed configuration. To assess the degree to which infinite swept conditions were achieved in the experiment, Dagenhart et al. [37] measured the pressure distribution on the upper wing surface at the upper end and bottom of the model, through pressure taps in the chordwise direction. Due to the measurement location being very close to the liner and minor asymmetries in the liner profiles on each end of the wing, it was noted by Dagenhart et al. [37] that the measurements did not fall on top of each other, but were otherwise expected to match the prediction from the MCARF airfoil code. The predictions from CFD match the airfoil code predictions. However, with the predictions from CFD bounding the measured data, it is not clear which pressure distribution one should use. The computed pressure distribution from the CFD solution was used as input to the BLSTA laminar boundary layer code [51] to generate accurate velocity profiles for linear stability analysis of the boundary layer. The LASTRAC [52] stability code was used to compute the envelope of the cross flow N-factors along the upper surface of both the free-air and the installed configurations. The stability analysis was based on the PSE, which account for the effects of both mean flow nonparallelism and surface curvature on the disturbance amplification rates. Computations were performed at streamwise chord Reynolds numbers of 2.37×10^6, 2.73×10^6, 3.27×10^6 and 3.72×10^6, respectively, and the predicted evolution of the N- factor envelopes in each of those cases is shown in Fig. 2(b). The selected Reynolds numbers correspond to the conditions at which Dagenhart et al. [37] carried out the initial experiments and at which cross flow effects were dominant. Figure 2(b) shows that, for each of the conditions, the installed configuration yields a slightly higher crossflow N-factor than the free-air configuration at any given streamwise location, consistent with the stronger favorable pressure gradient seen on the upper surface of the installed wing in Fig. 2(a).

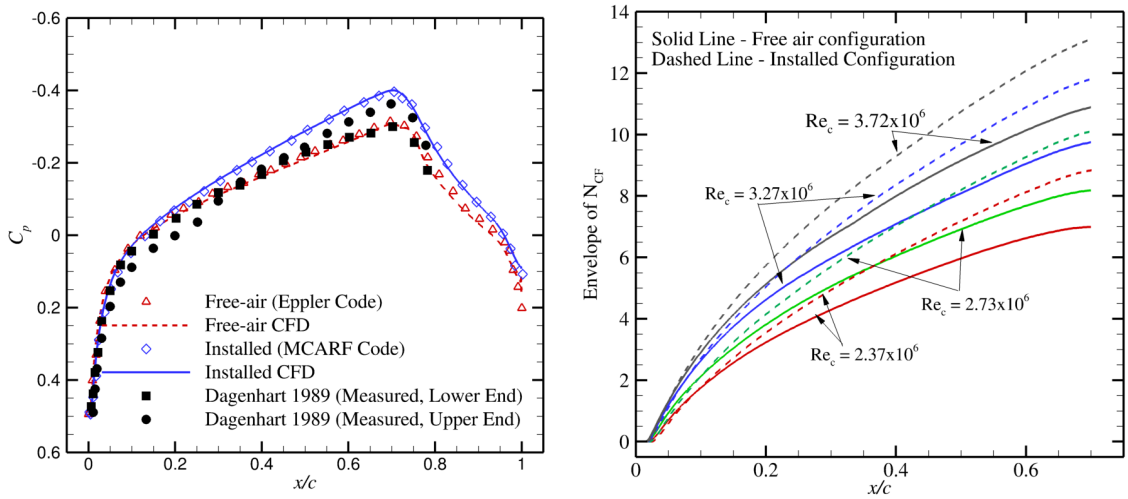

(a) Pressure distribution on the upper surface of the swept wing

(b) Envelope of crossflow *N*-factors from linear stability analysis

Fig. 2. Pressure distribution and the crossflow N factor envelops for the NLF(2)-0415 swept airfoil experiment in free-air and installed configuration.

As mentioned in Section II, the Langtry-Menter transition models (LM2009 and LM2015) are supposed to be implemented with the SST 2003 turbulence model, but the calibration of LM2015 reported by Langtry et al. [32] was done based on an implementation with the baseline version of the SST model as its underlying turbulence model. Furthermore, the initial verification of the LM2015 model implementation in the OVERFLOW 2.2o code was based on the free-air configuration. It also deserves mentioning that, all of the data from the experiment by Dagenhart et al. [37] that were used for model calibration and evaluation by Langtry et al. [32] (see data points corresponding to $k = 3.3$ μm in Fig. 4 from Ref. [32]) appear to be shifted to the left along the Re_c axis by approximately 0.2 x 10^6, with the last data point being at Re_c =3.5 x 10^6 instead of at Re_c =3.72 x 10^6. One possible reason for this inadvertent shift may be that these data came from Fig. 4 from the earlier paper by Radeztsky et al. [38] that had the same shift while plotting the effects of surface roughness and flow Reynolds number on the transition location. Since the flow conditions of the Dagenhart et al. [37] experiment were clearly outlined in their paper, we will assume those conditions represent the correct values for the case of $k = 3.3$ μm. Also, the computations for this case were carried out by Langtry et al. [32] with an assumed freestream turbulence intensity of 0.2%, which is different from the actual value (0.09%) in the wind tunnel as described in Ref. [39].

Due to the various reasons mentioned above, as a first step in evaluating the LM2015 transition model, we repeat the computations for the swept wing using both the free-air and the installed configurations. The computations are done at the chord Reynolds numbers mentioned earlier for all of the levels of surface roughness from the experiments. Results from the computations are also expected to reveal if recalibration of the LM2015 model is needed. Although, the LM2009 and AFT2017b models cannot predict crossflow effects, those were also invoked for the sake of completeness. The transition locations were determined from the skin friction distributions obtained from the CFD computations, by drawing a tangent to the laminar portion of the C_f vs. x/c curve at the location where it begins to rise and determining if this tangent intersects the tangent at the midpoint between the laminar and turbulent skin friction values. Alternatively, a turbulence index, originally proposed by Spalart [43, 53], value of 0.5 or an intermittency (γ) value of 0.03 could also be used to determine the transition location. Given the similarity between the predictions of the AFT2017b and LM2009 models for the NLF(2)-0415 swept wing, only results from the predictions of the AFT2017b model are shown in Fig. 3(a) along with the results from the LM2015 model. As expected, the AFT2017b (and also the LM2009) model fails to capture the earlier onset of transition due to crossflow effects. In comparison, the LM2015 model predictions for the transition locations over the free-air configuration are closer to experimental measurements at three roughness levels. However, these results appear to be slightly different from those obtained by Langtry et al. [32] (see Fig. 4 in Ref. [32]), especially for the case of k = 0.25 μm, possibly due to the effects from the SST-2003 turbulence model and the shift in data for $k = 3.3$ μm. Interestingly, Fig. 3(b) indicates a relatively poor comparison between the predictions based on the

installed configuration and the experimental measurements. Although computations of linear disturbance growth predicts a higher N_{CF} factor for the installed configuration (see Fig. 2(b)), suggesting earlier transition than the free-air configuration, the trend based on the prediction by the LM2015 model appears to be in the opposite direction. This could be indicative of the crossflow model not accounting for the strengthened crossflow due to stronger favorable pressure gradients over the installed configuration. It could also be indicative of the need for recalibrating the transition model.

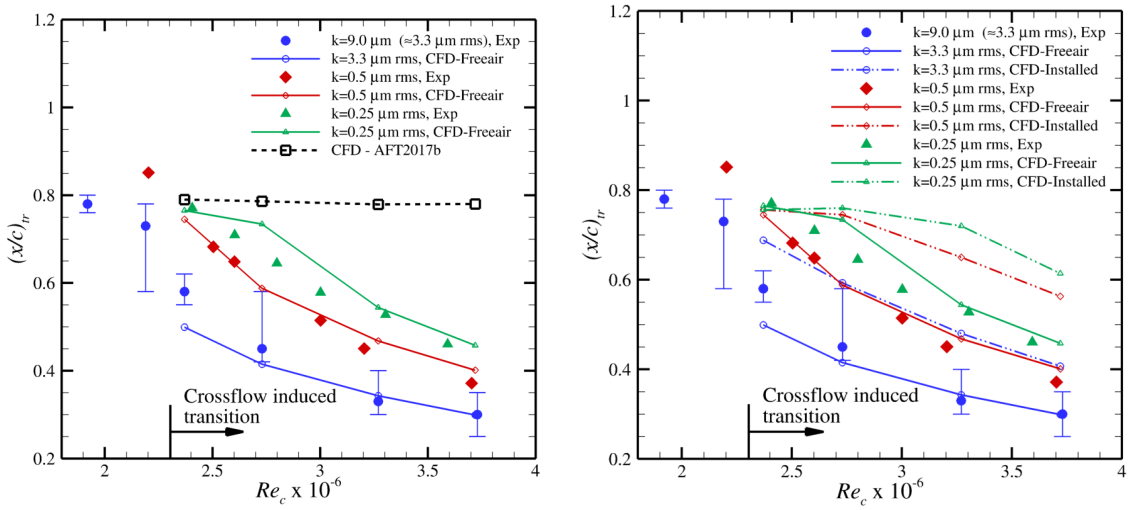

(a) LM2015 vs. AFT2017b free-air **(b) LM2015 free-air vs. installed**

Fig. 3. Comparison of predicted and measured transition front for various roughness levels, with CFD computations performed in free-air or installed configurations.

1. LM2015 Model sensitivity to grid spacing

Continuing with the evaluation of the LM2015 transition model, the sensitivity of this model to both chordwise and wall-normal grid resolutions of the OVERFLOW computations was characterized. To study the dependence on chordwise resolution, computations were performed for several grids containing 301, 425, 601, 851 and 1201 points, around the airfoil, while the wall normal spacing was fixed at $y^+ = 0.125$. As long as there were more than 223 points on each side of the wing, the transition location based on skin friction distribution did not vary by more than 1% of chord length, and hence those are not shown here. For the study on the potential sensitivity to the wall normal resolution, the chordwise resolution was fixed at 601 points around the airfoil and the near wall grid spacing at 10% chord was varied from $y^+ = 0.0625$ to 1.0, with a two fold increase at every step. The computations were carried out for all three of the surface roughness levels at $Re_c = 3.72 \times 10^6$, and the results of those are shown in Fig. 4. On the scale of this figure, the C_f distributions nearly collapse onto each other as long as $y^+ \leq 0.25$.

2. Recalibration of the LM2015 model

In the original formulation of the LM2015 model, a correlation for the SCF induced transition onset momentum thickness Reynolds number, $(Re_{\theta t})_{SCF}$, as a function of the surface roughness level was estimated by following the approach of Crouch and Ng [48]. Crouch and Ng [48] had determined a relation between N_{CF} and the nondimensional root-mean-square amplitude of the surface roughness, where the roughness amplitude was scaled with respect to the streamwise boundary layer displacement thickness at the neutral point of the critical crossflow mode, i.e., the most amplified crossflow disturbance at the transition location. Langtry et al. [32] obtained a similar correlation for $(Re_{\theta t})_{SCF}$ in place of N_{CF} by using a logarithmic fit for the data from the NLF(2)-0415 45° swept wing experiment. Then, to account for differences in cross flow strengths (H_{CF}) relative to the NLF(2)-0415 experiments, additional data from computational data based on stability analyses for the NLF(2)-0415 airfoil at other sweep angles (i.e., both larger and smaller than 45°) as well as data from experiments on a prolate spheroid were used to characterize the resulting shift in the $(Re_{\theta t})_{SCF}$.

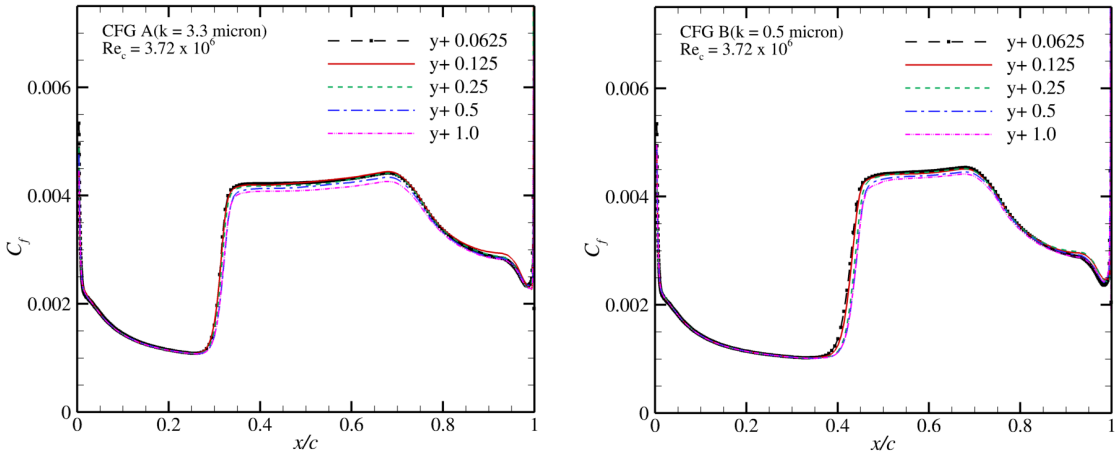

(a) $k = 3.3\ \mu$m **(b) $k = 0.5\ \mu$m**

Fig. 4. Sensitivity of the LM2015 model to wall normal grid spacing.

The computed value of $(Re_{\theta t})_{SCF}$ was used in a sink term from the $Re_{\theta t}$ equation in order to account for the onset of crossflow induced transition. For reference, the correlation obtained by Langtry et al. [32] is given below.

$$(Re_{\theta t})_{SCF} = \frac{\rho\theta_t(\frac{U}{0.82})}{\mu} = -35.088\ ln\left(\frac{k}{\theta_t}\right) + 319.51 + f(+\Delta H_{CF}) - f(-\Delta H_{CF}). \quad (1)$$

The last two terms on the right side of Eq. 1, represent the shifts needed to account for changes in the crossflow strengths relative to that in the NLF(2)-0415 45° swept-wing experiment. Their complete formulation can be found in Ref. [32]. The initial recalibration effort reported here is limited to this experiment, and hence the shift terms in Eq. 1 will not be altered in this paper. A future effort will address recalibration of those shifts by using additional configurations with different levels of crossflow. For each of the Reynolds numbers and surface roughness levels (for both the free-air and the installed configurations), the boundary layer profiles from the BLSTA code and the envelope of the N_{CF} curves obtained from stability analysis based on PSE are used to determine details about the boundary layer such as the momentum thickness at the neutral point of the critical crossflow mode and at the transition location, and the edge conditions at the transition location (density, velocity and viscosity). Using the newly obtained data, the nondimensional rms amplitude of the surface roughness (k/θ) and $Re_{\theta t}$ are computed. Then a new curve fit is obtained for $(Re_{\theta t})_{SCF}$ vs. $\left(\frac{k}{\theta}\right)$ for the data points shown in Figs. 5(a) and (b). The new curve fit for the free-air configuration is

$$(Re_{\theta t})_{SCF} = \frac{\rho\theta_t(\frac{U}{0.78})}{\mu} = -32.291\ ln\left(\frac{k}{\theta_t}\right) + 326.157 + f(+\Delta H_{CF}) - f(-\Delta H_{CF}). \quad (2)$$

Whereas the fit for the installed configuration involves somewhat different values of the numerical coefficients, as given by

$$(Re_{\theta t})_{SCF} = \frac{\rho\theta_t(\frac{U}{0.75})}{\mu} = -31.176\ ln\left(\frac{k}{\theta_t}\right) + 294.87 + f(+\Delta H_{CF}) - f(-\Delta H_{CF}). \quad (3)$$

As mentioned earlier, the terms $f(+\Delta H_{CF})$ and $f(-\Delta H_{CF})$ from Eqs. 2 and 3 have been kept the same as those in Ref. [32]. The newer results from the model recalibrated within the limited setting of the NLF(2)-0415 45° swept wing experiment are shown in Figs. 6(a) and 6(b). The effect of surface roughness and chord Reynolds number on the predicted transition location is shown in these plots. In the case of free-air configuration, for each of the Reynolds numbers at which the computations were carried out, see Fig. 6(a), it can be seen that the downstream shift in the predicted transition location with reduced roughness levels is

captured correctly and matches the measured locations. Prior to recalibration, the predicted transition location for Re_c = 2.73 x 10^6, 3.27 x 10^6, and 3.73 x 10^6 with k = 0.5 μm and 0.24 μm (see Fig. 3(a)) was further downstream than the measured location for this configuration. For the installed configuration, as observed from Fig. 6(b), the predictions from the recalibrated model now lies within the experimental bounds for k = 3.3 μm at all Reynolds numbers, as opposed to the results before the recalibration when they were far downstream of the measured location (see Fig. 3(b)). The comparison for the other two surface finishes (k = 0.5 μm and 0.24 μm) is better than prior to recalibration, but still far downstream of the measured locations. It is not clear, if this is due to the curve fit purely relying on the surface finish instead of also accounting for the pressure gradients and needs to be investigated further. However, we believe that it is more important to broaden the database by acquiring comparable data for other configurations for which the transition process is dominated by the stationary crossflow instability. In passing, we also note the need to extend the correlation by including additional parameter(s) related to the freestream turbulence in the transition correlations analogous to Eqs. 1 to 3.

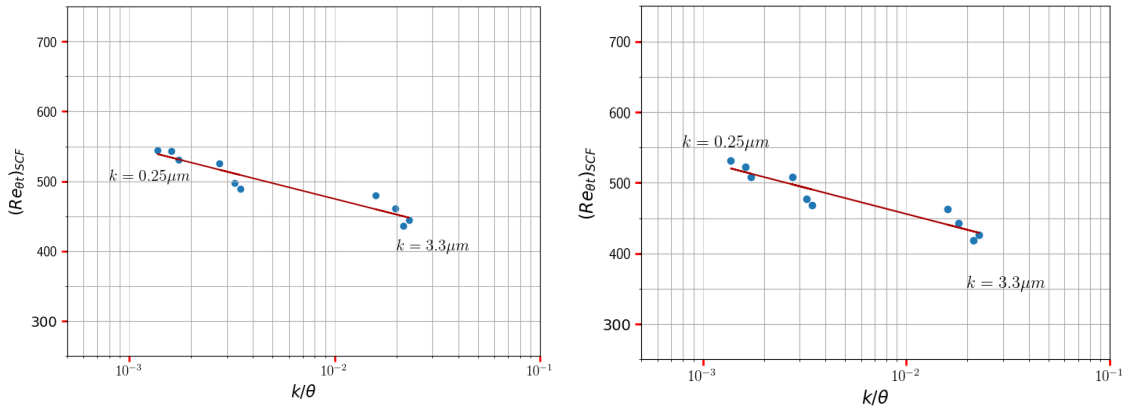

(a) Free-air configuration **(b) Installed configuration**

Fig. 5. New empirical correlation for stationary crossflow based on NLF(2)-0415 experiment.

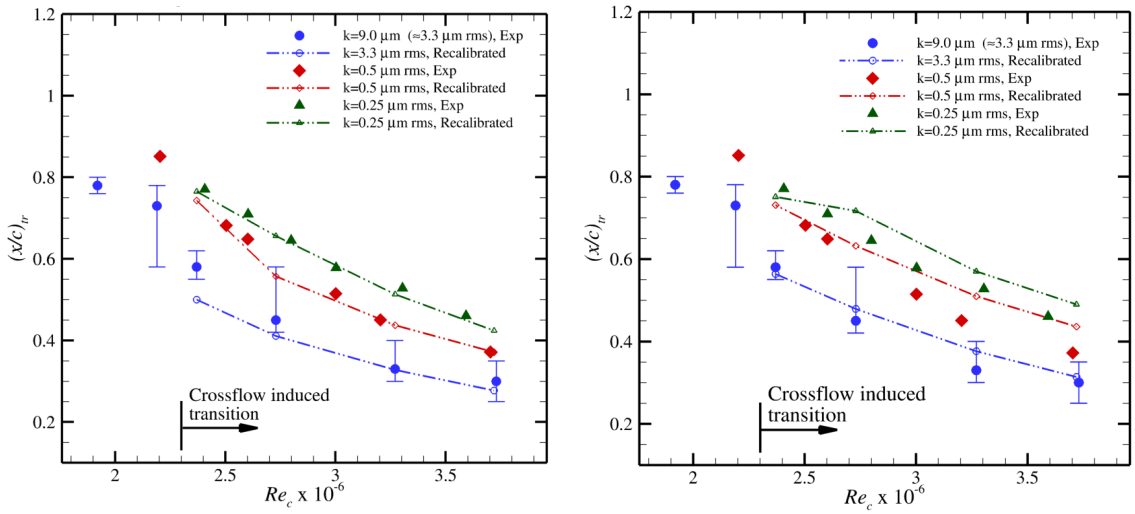

(a) Free-air configuration **(b) Installed configuration**

Fig. 6. Comparison of measured transition front against predictions from recalibrated LM2015 model for free-air and installed configuration.

B. Technical University of Braunschweig Sickle Wing

The sickle wing transition experiment by Petzold and Radespiel [40] is well-suited for the assessment of the transition models for cross flow induced boundary layer transition over fully three-dimensional swept-wing configurations. The wing consists of four sections with varying sweep angle, as shown in Fig. 7, making the flow highly three-dimensional with strong spanwise gradients, that may pose challenges for transition prediction based on the simpler models for instability growth such as the classical, quasiparallel stability theory without any effects of surface curvature. More details on the complete specification of the wing model can be found in Ref. [40]. The angle of attack and Reynolds number were varied during the experiment, allowing the measurements to cover a wide range of transition scenarios, including TS, CF, and mixed-mode transition. The transition fronts on both top and bottom surfaces of the wing model were obtained via infrared thermography. To help evaluate the transition models in OVERFLOW, computations were performed for three different test conditions, including the original test condition from Ref. [40] and two other test conditions that were also provided to the participants of the AIAA SciTech 2018 special session titled "*CFD Transition Modeling and Predictive Capabilities*" [54]. The above set of conditions are summarized in Table 1. For these three test conditions, interference effects from the wind tunnel side wall were deemed to be low, so the wind tunnel walls are not included in these computations. The freestream turbulence intensity was set to the tunnel value of 0.17%. The surface roughness was measured in the experiment to have an rms height of 1.47 μm and a five-point average of the maximum peak to peak height of 9.78 μm. The measured transition front on the upper and lower surfaces of the wing and the pressure distribution on sections of the wing from the experiment were also provided to the participants of the AIAA SciTech 2018 special session.

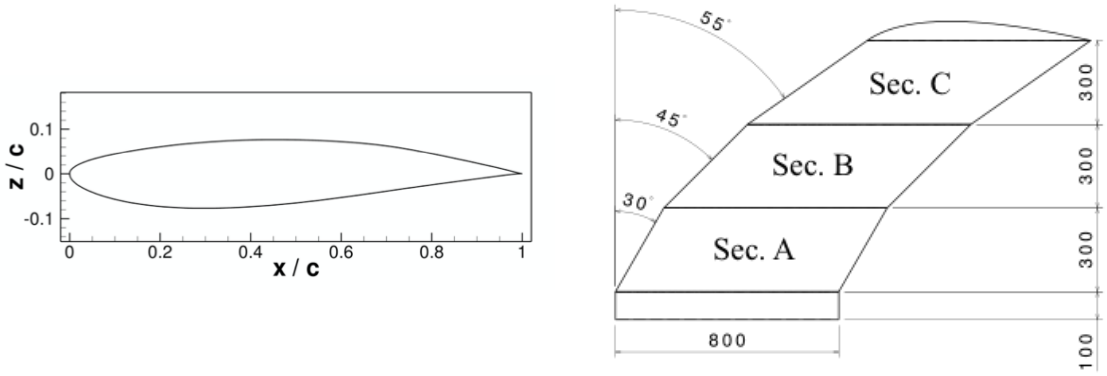

Fig. 7. Sketch of the sickle wing cross section and the model planform (all dimensions in mm) [40].

Table 1. Test conditions for the sickle-shaped wing experiment by the Technical University of Braunschweig.

Case	A	B	C
Mach number	0.156	0.259	0.259
Angle of attack	-2.6°	-2.6°	-0.3°
Reynolds number	2.75 x 10^6	4.45 x 10^6	4.43 x 10^6
Reference temperature (°C)	22.62	28.38	28.98
Reference pressure (Pa)	98919	98974	103614

A C-grid with a wake cut on the trailing edge was generated for the near-body grid using CGT [50]. The generation of off-body grids and hole-cutting were carried out by using OVERFLOW's domain connectivity

function (DCF) approach. The baseline grid, which was used for most of the results shown herein, had a near-wall spacing of $y^+ = 0.33$, based on the conditions at midchord, and has approximately 497 points around the wing in the chordwise direction and 233 points in the spanwise direction with clustering around the location of sweep changes.

Figures. 8(a), (b), and (c) display the respective contours of the turbulence index for case A obtained using the AFT2017b, LM2009 and original LM2015 models, respectively. Contour value of 0.5 was generally recommended to indicate the start of transition, while values close to zero (i.e., the blue shaded regions) indicate the laminar region. Hence, in each of these figures, the upper limit of the contour values was fixed at 0.5. On the lower surface of the wing, which was found to be dominated by TS induced transition in the experiment, all three models appear to perform well in regards to comparison with the measured transition front, which is also marked by the black curve in each of these figures. In terms of their relative performance, the LM2015 and AFT2017b models predict a slightly earlier transition on the lower side in comparison with the measurements, whereas the predicted transition front by the LM2009 model (start of red color region in turbulence index contour plot indicating contour values ≥ 0.5) is closely aligned with the measured transition front. Transition over the upper surface of the wing was dominated by the TS effects within section A, while crossflow effects appeared to dominate behind the rapid change in sweep from section A to section B, and in most of section C. Based on the zig-zag pattern of the transition front from the experiment, transition over section B could include both TS and CF mechanisms. All three models appear to provide quite accurate predictions of the transition front within section A, while only the LM2015 model is able to predict the transition front almost correctly within the outboard segments of the upper surface by virtue of its ability to model crossflow transition. The predicted transition front by the LM2009 and the LM2015 models are comparable to other computations performed using variants of the LM2009 model in Ref. [34]. Figures. 9 (a) and 9(b) also show that the surface pressure distributions predicted by all three models agree well with the measured pressure coefficients along the midspan of each of the wing sections A, B, and C.

1. Sensitivity of LM2015 Model predictions to grid spacing

The sensitivity of the transition front predictions based on the LM2015 model to grid spacing in all three directions was studied by systematically varying one of them while keeping the other two fixed. The results from this study are shown in Fig. 10. During the first part of this study, the wall normal grid spacing was varied by reducing it from its value for the baseline grid ($y^+ = 0.33$) to $y^+ = 0.1$ or by increasing it to $y^+ = 0.5$, while retaining the number of points in the chordwise and spanwise directions at 497 and 233 respectively. A comparison between Fig. 10(a) and Fig. 8(c) indicates that, for this specific configuration, the transition predictions based on the LM2015 model exhibits a rather low sensitivity to the near-wall grid spacing. As a follow-on to varying the wall-normal grid spacing, the chordwise resolution was changed from 497 to either 351 or 701, while retaining the wall normal spacing at the intermediate value of $y^+ = 0.33$ and the spanwise resolution at 233, and the turbulence index contours based on this variation are plotted in Fig. 10(b). Finally, the spanwise resolution was increased from 233 to either 331 or 467 as suggested in Ref. [54], while retaining the wall normal spacing at $y^+ = 0.33$ and the chordwise resolution at the intermediate value of 497 points along the airfoil contour. The results of this computation are shown in Fig. 10(c). The predicted transition front appeared to be very robust to all of these grid variations, indicating that the baseline grid was adequate for this study.

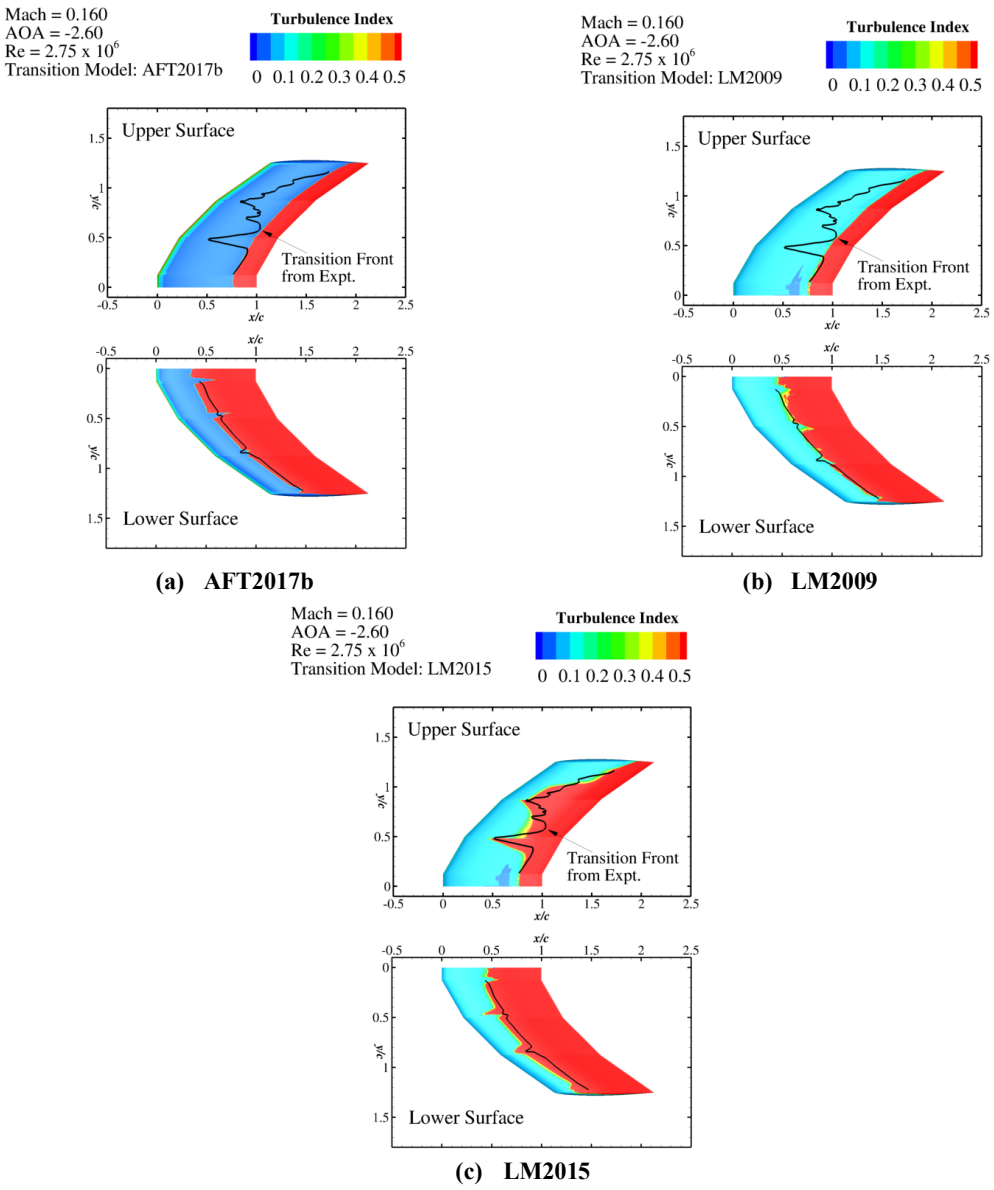

Fig. 8. Measured and predicted transition front for the sickle wing experiment at flow conditions corresponding to case A. The prediction is depicted via turbulence index contours for selected transition models.

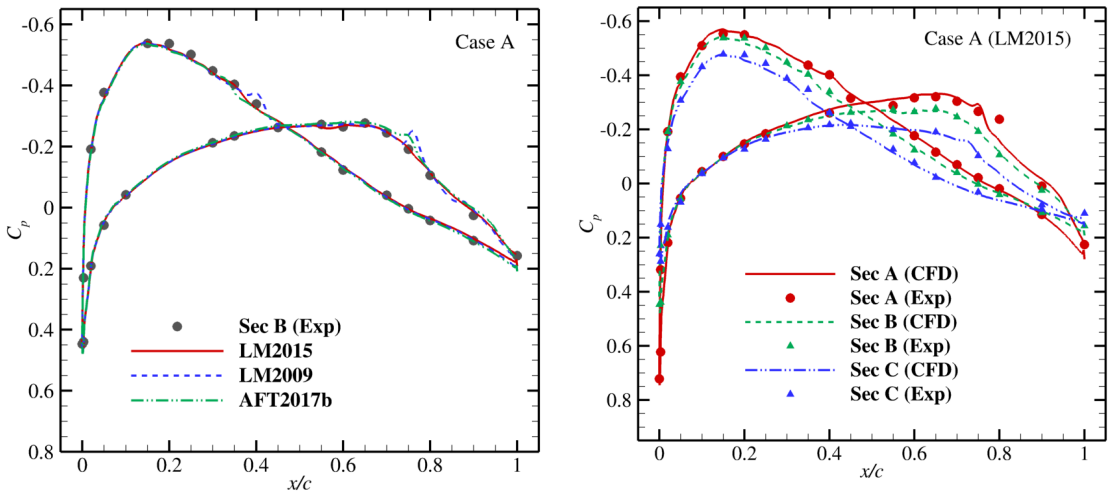

(a) Pressure coefficient at midspan region of section B

(b) Pressure coefficient at the midspan region of all sections

Fig. 9. Predicted and measure pressure coefficient for the sickle wing experiment using various transition models for case A.

2. Sensitivity of transition model performance to flow conditions

The sensitivity of the various models to flow conditions was evaluated by running the AFT2017b, LM2009 and LM2015 models with flow condition listed for cases B and C in Table 1. The computations were carried out with the grid having a wall-normal spacing of $y^+ = 0.1$, as a precaution, given the increased Reynolds number. As both AFT2017b and LM2009 models only address TS mode of transition, only results from AFT2017b and LM2015 are shown here for brevity.

As case B corresponds to higher Reynolds number but the same angle of attack as case A, the crossflow effects over the upper surface are expected to be stronger for case B. This is confirmed by the significant upstream movement of the measured transition front inside sections B and C on the upper surface of the wing, as seen from Fig. 11 (a) and (b). Section A of the upper surface and sections A to B of the lower surface of the wing continues to be dominated by TS effects. Perhaps not surprisingly, until the midspan of section A on the upper surface, AFT2017b does well, while the LM2015 model seems unable to capture the sharp jump in the measured transition front near the region between sections A and B. On the lower surface, the AFT2017b model predicts the transition front correctly until section B, while the LM2015 model also does well with the exception of indicating a slightly earlier transition. However, the LM2015 model does capture the crossflow effects indicated by the zigzag pattern in the transition front over section C of the lower surface that is missed by the AFT2017b model. On the upper surface, only the LM2015 model is able to correctly capture the crossflow induced upstream shift in the transition front in comparison with the predictions based on the other two models that are restricted to TS transition alone.

The final test condition, i.e., condition C from Table 1, involved a reduced angle of attack and was intended to create a more TS dominated transition on the upper surface of the wing. The effects of this change may be observed in Figs. 11(c) and 11(d) from a downstream shift in the transition front over portions of section B of the upper surface in relation to the transition front from the test condition B discussed in the preceding paragraph. The biggest change, however, is that the lower surface now includes a larger region of crossflow dominated transition, and therefore, resembles the transition behavior over the upper surface in case B. Given the relative dominance of crossflow effects on both the lower and upper surfaces, the LM2015 model does well in predicting the transition front in this case on both the upper and lower surface of the wing. As indicated by Figs. 12(a) and 12(b), the pressure coefficient predictions by the LM2015 model (obtained at the midspan of each of the wing segments) agrees well with those measured during the experiment for test conditions B and C. Although not shown here, pressure coefficients obtained using LM2009 and AFT2017b also compared well against measurements for test conditions B and C.

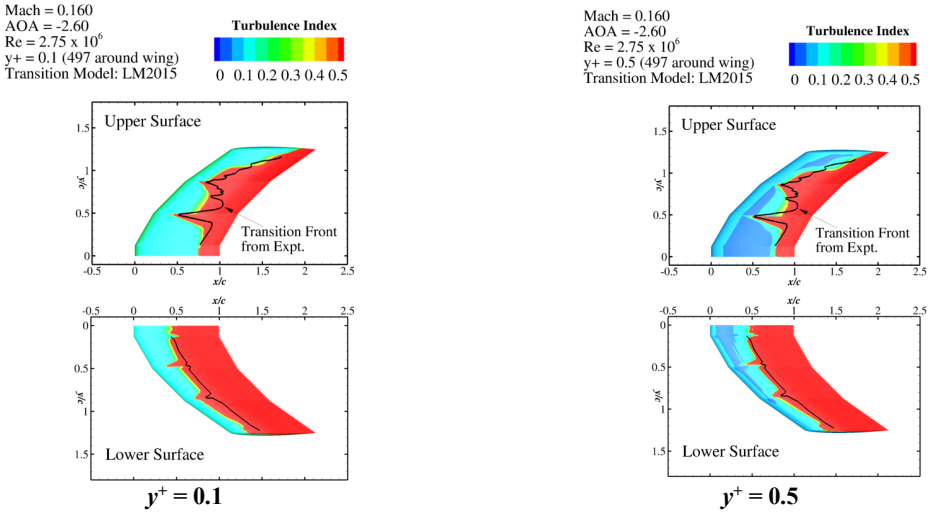

$y^+ = 0.1$ $y^+ = 0.5$

(a) Wall-normal spacing variation

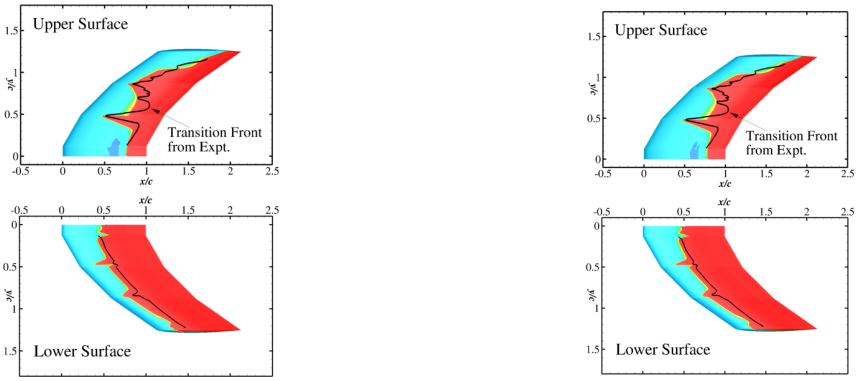

351 points **701 points**

(b) Chordwise grid resolution

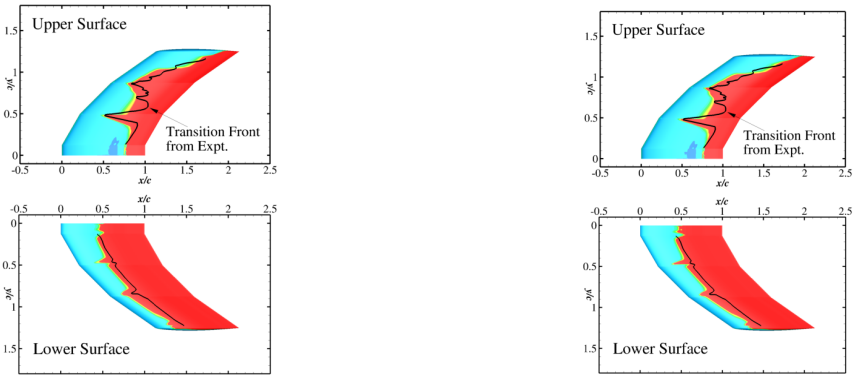

331 points **467 points**

(c) Spanwise grid resolution

Fig. 10. Sensitivity of the LM2015 model to grid spacing in predicting the transition front for the sickle wing experiment at flow conditions corresponding to case A.

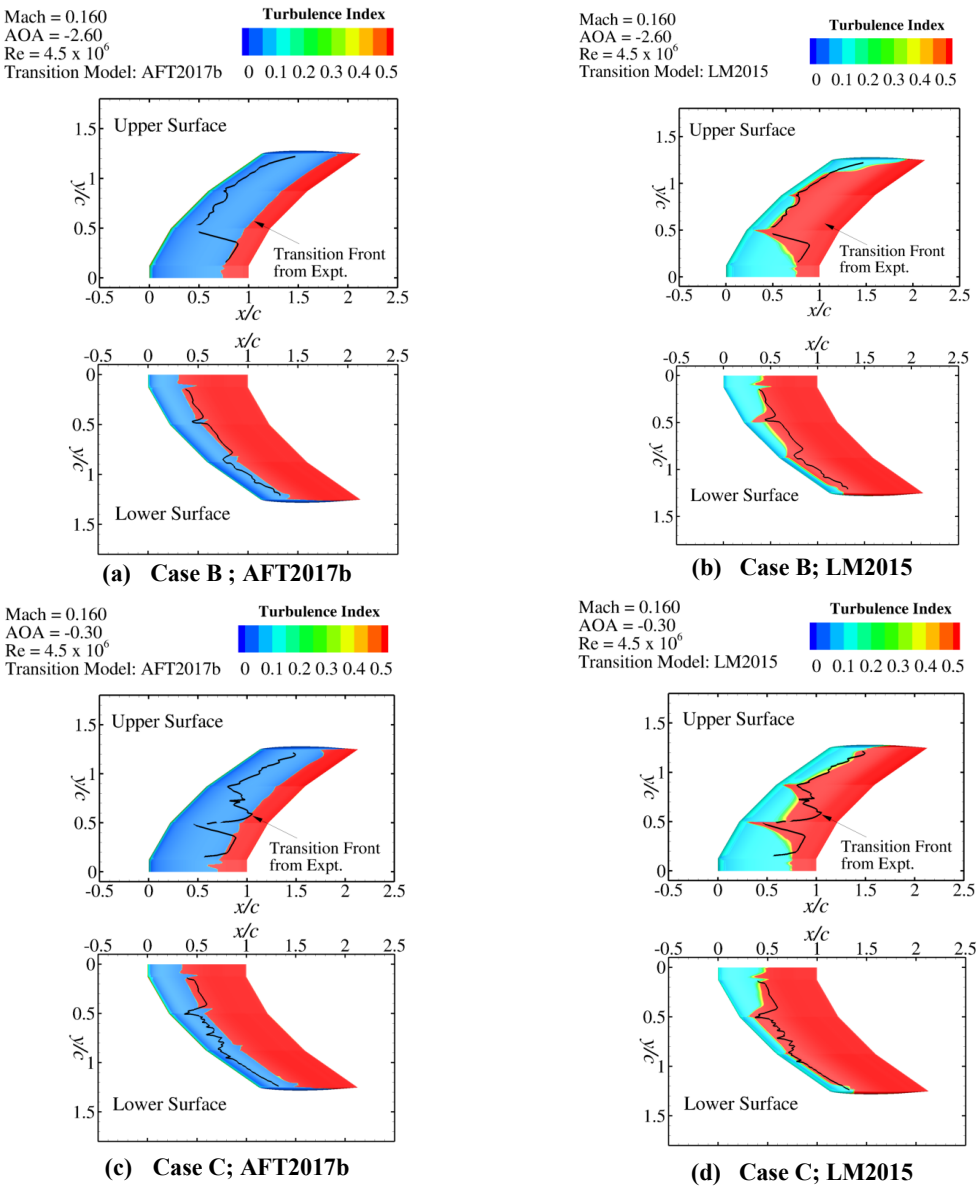

Fig. 11. Measured and predicted transition front for the sickle wing experiment at flow conditions corresponding to cases B and C.

3. Recalibrated LM2015 model

Results obtained with the recalibrated LM2015 models, based on Eqs. (2) and 3, respectively (i.e., based the on the NLF(2)-0415 swept wing data for the free-air and installed configurations, respectively) are shown in Figs. 13(a) and 13(b). Figures 13(a) and 13(b) indicate that, the results from both recalibrated versions of the LM2015 model do not differ much and closely resemble the measured transition front from the experiment. There is a small upstream movement of the predicted transition front on section B of the upper surface, for the recalibrated LM2015 model based on the installed configuration of NLF(2)-0415. However, as mentioned earlier, the current recalibration does not account for the shift terms that would be activated by the differences in crossflow strength between the sickle wing case and the NLF(2)-0415 configuration with a sweep angle of 45 degrees. Thus, evaluation of the recalibrated models will be repeated in the future, after the impact of variation in the crossflow strength has been accounted for.

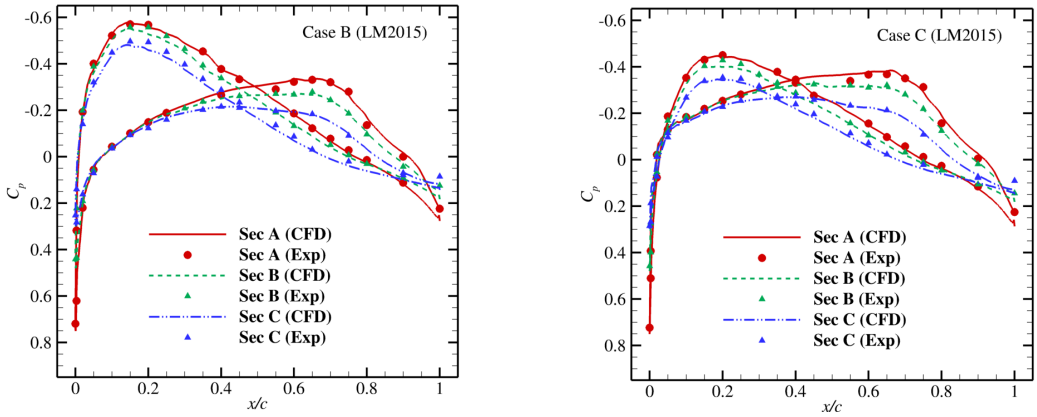

(a) Case B **(b) Case C**

Fig. 12. Predicted and measured pressure coefficient for the sickle wing experiment using the LM2015 model for cases B and C.

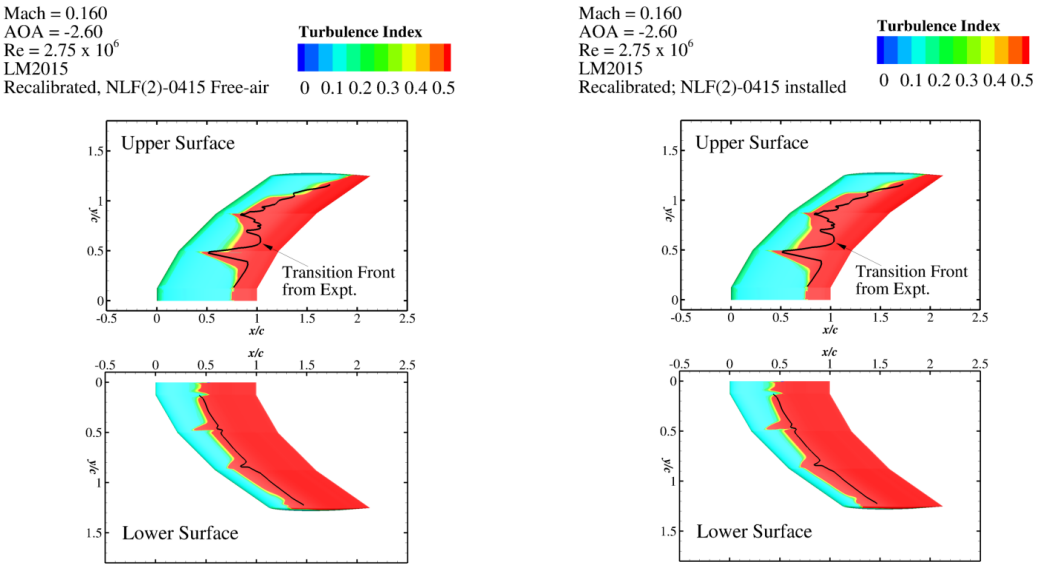

(a) Recalibrated for NLF(2)-0415 free-air configuration **(b) Recalibrated for NLF(2)-0415 installed configuration**

Fig. 13. Comparison of the predicted transition front by the recalibrated LM2015 model with the measured front for the sickle wing experiment at flow conditions corresponding to case A.

C. Wing-Body CRM configuration

As a precursor to the study of the CRM-NLF configuration, the CRM wing-body configuration from the Fourth and Fifth AIAA Drag Prediction Workshop [41] was chosen as one of the test cases to evaluate the transition models and to compare the transition predictions based on the different models within a fixed flow solver. Analogous comparisons with the NASA unstructured flow solver FUN3D [55] are planned during a follow-on study. The CRM computations were initially run at the specified conditions of Mach 0.85 and a Reynolds number, based on the mean aerodynamic chord, equal to 5×10^6. The angle of attack was held fixed at 2.195°. Given that the recent experiments on the CRM-NLF were carried out at $Re_c = 15 \times 10^6$, an additional run was also performed at the higher Reynolds number, while maintaining the Mach number at 0.85. It is to be noted that the CRM wind tunnel experiments employed transition dots that resulted in a turbulent flow approximately everywhere [41]. As a result, there is no experimental data to evaluate the

accuracy of the transition models for this particular test case. However, given the low-to-moderate Reynolds numbers, these flow conditions allow for a significant region of laminar flow in the absence of the trip dots, and therefore, the CRM serves as a useful means toward a limited assessment of the transition models, especially in the context of a typical wing design that does not include the natural laminar flow features.

The grid used for the $Re_c = 5 \times 10^6$ computations corresponds to the extra fine grid from the family of unified baseline grids provided for the Fourth and Fifth AIAA Drag Prediction Workshop [56],[§§] which contained approximately 43 million grid points with a resulting y^+ of approximately 0.5 in the midchord region. For the $Re_c = 15 \times 10^6$ run, the super fine grid provided for the workshop was used. The super fine grid contained approximately 143 million grid points with a resulting y^+ of approximately 0.33, based on $Re_c = 5 \times 10^6$, but a higher value of $y^+ = 1.0$ for $Re_c = 15 \times 10^6$. The free stream turbulence intensity was prescribed to be 0.24%, based on the previous characterization of the NTF tunnel [57] and the surface roughness of the model was specified to be 1 μinch, equal to that measured on the CRM-NLF model [28].

The computations were performed with the AFT2017b, LM2009, and the LM2015 transition models (the later without the recalibration discussed earlier in this paper). As there was no significant difference between the results obtained via the LM2009 and LM2015 models, respectively, only the results from the LM2015 model are shown. To provide a visual understanding of the transition fronts predicted by the AFT2017b and LM2015 transition models, Figs. 14(a) and 14(b) display the respective contours of the turbulence index. Both models indicate the flow being fully turbulent near the wing root. Away from the wing root region, and until the Yehudi break, a substantial region of laminar flow is indicated with the LM2015 model, whereas a significantly smaller laminar acreage is predicted by the AFT2017b model. The change in laminar acreage on this portion of the wing also appears to reflect upon the pressure distribution on the upper surface of the wing (see Fig. 15(a)), with a small jump occurring between $0.25 \leq x/c \leq 0.35$ for the AFT2017b model and between $0.4 \leq x/c \leq 0.5$ for the LM2015 model. The locations at which the pressure distribution is shown in Fig. 15 is indicated in Fig. 14(a). Outboard of the Yehudi break, the laminar region appears to extend up to the shock location with very little difference between the two models. The pressure distributions on the upper and lower surfaces of the wing obtained from the computations performed with the two models (see Figs. 15(b) and 15(c)) also closely match each other until the shock region. Finally, it is interesting to observe that near the nose region of the fuselage, the LM2015 (and also LM2009) model predicts a significantly larger laminar region than the AFT model. These results are consistent with the computations performed by Coder and Maughmer [22] for the same flow condition, but by using the medium grid from the sequence of grids provided at the AIAA Drag Prediction Workshop. A linear stability analysis was performed on the laminar portions of the baseflow state obtained for the specified conditions and the results indicated the amplification of both stationary and traveling crossflow modes within the inboard region; however, the *N*-factor values in the outboard section were rather modest, supporting the conjecture by Coder and Maughmer [22] concerning the boundary layer separation as the primary driver for transition within the outboard region.

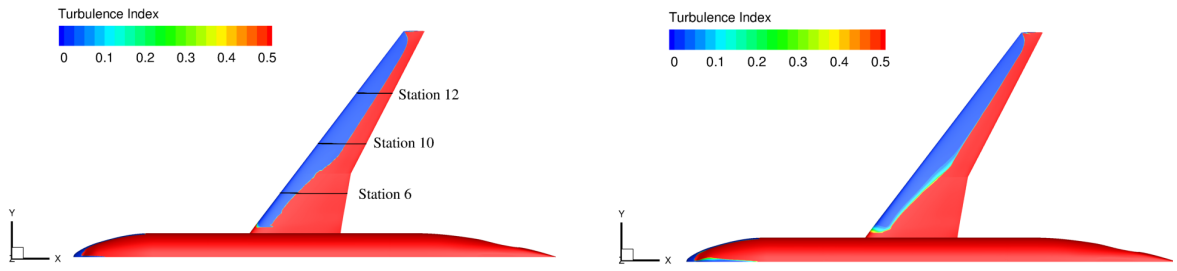

(a) AFT2017b Model **(b) LM-2015 Model**

Fig. 14. Comparison of the predicted transition behavior on the suction surface of the wing shown using turbulence index contours for $Re_c = 5 \times 10^6$.

[§§] https://dpw.larc.nasa.gov/DPW5/overset_grids.REV01/ (last accessed: Nov 19, 2019)

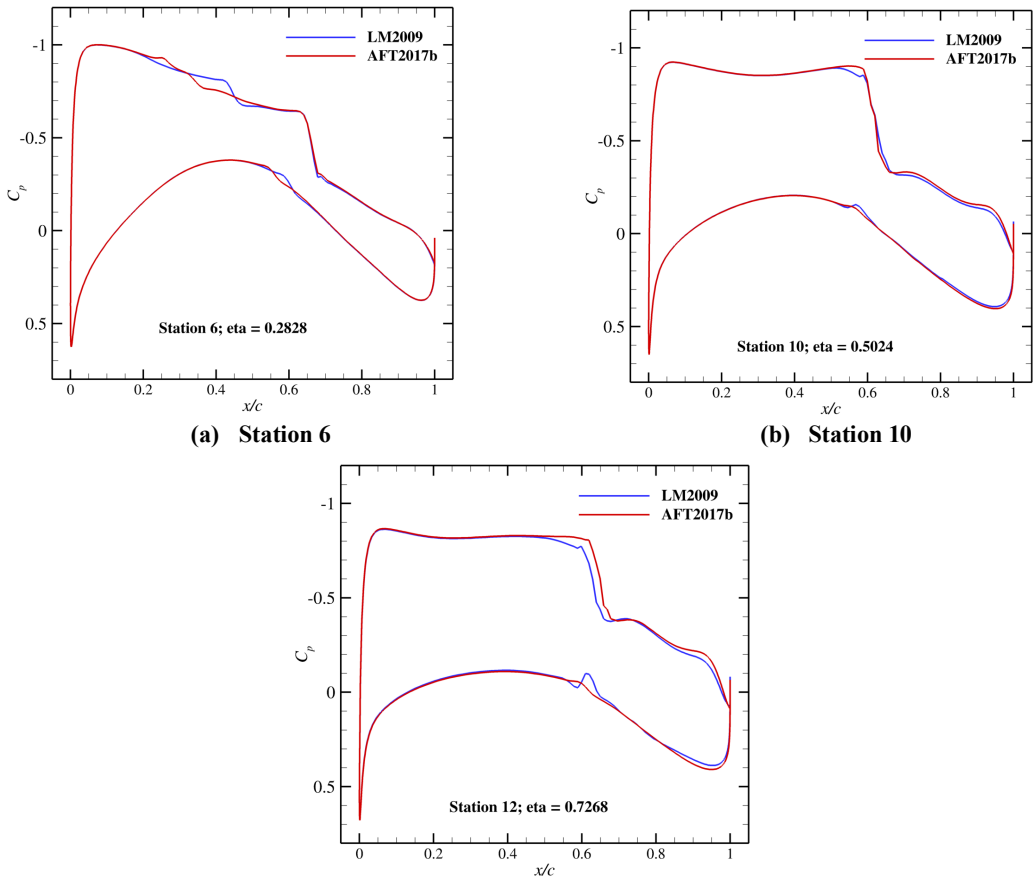

(a) Station 6 **(b) Station 10**

(c) Station 12

Fig. 15. Computed pressure distributions at various stations on the CRM wing obtained using various turbulence/transition models for α=2.195° and $Re_c = 5\times10^6$.

As the recent CRM-NLF experiments were carried out at higher Reynolds numbers (between 10×10^6 – 30×10^6 based on the mean aerodynamic chord), additional computations were performed for the same angle of attack and Mach number, but at a $Re_c = 15 \times 10^6$, as mentioned earlier. Given the lack of experimental data to assess the performance of the transition models under this flow condition, linear stability analysis was carried out yet again to provide some estimates of the N-factors at the transition fronts predicted by the transition models. Linear stability analysis based on PSE that also accounted for nonparallel flow and curvature effects were carried out on the laminar portions of the computed baseflow, using LASTRAC [52]. It is important to note that the baseflow was computed on the same super fine grid from the family of unified grids. Although this grid was not the ideal grid from a stability analysis perspective (due to the number of points within the boundary layer and the growth rate of wall-normal spacing within the critical region of the boundary layer), it was still a reasonable one for the purpose of preliminary assessment.

Shown in Fig. 16 is a contour plot of the pressure distribution over the upper surface of the wing, superimposed with N-factor values for critical modes at a select few locations obtained from the linear stability analysis. Slightly away from the root of the wing, the TS modes do not show a significant growth in amplitude ($N_{TS} \approx 2$). However, as one approaches the Yehudi break, both TS and crossflow modes undergo significantly higher amplification ($N_{TS} \approx 6$; $N_{CF} \approx 8$). As one moves away from the break, until the tip of the wing, only the TS modes remain significant. The TS modes reach N-factors of about 7 far upstream of the shock location in the regions just beyond the break, while they get close to the shock location as one nears the wing tip. Based on this analysis, crossflow is not expected to play a significant role for this flow condition,

so both the AFT2017b and LM2009/LM2015 models are applicable to the transition scenarios on this wing. As seen from Fig. 17, both models predict that the laminar regions shrink substantially in relation to the results presented previously for the lower Reynolds number case. However, there is still a substantial difference between the predictions of the AFT2017b and the LM 2015 models, with the AFT model appearing to predict a much earlier onset of transition across the wing span. Maximum *N*-factor computed using LST at the front predicted by AFT2017b appear to be very small (see Fig. 17(a)) to indicate onset of boundary layer transition. The predicted transition front from the LM2015 model does match the location of maximum *N*-factor predicted by LST on the outboard sections of the wing, as shown in Fig. 17(b). But, as one moves inboard towards the root of the wing, both models perform poorly. LST does indicate very small values of N_{TS} in this region, hence, one should be able to sustain a larger laminar region. Whether this is due to the turbulent state of the boundary layer coming from the fuselage, or due to some other factor is not clear at this stage. As for the poor prediction from the AFT2017b, it could be argued that the higher speed of this particular flow may have played a role, given that the model relies heavily on the correlations based on incompressible flows and may not have accounted for the increased boundary layer stability due to compressible effects. Additional data from the CRM-NLF experiment, may help us assess the above aspects of the AFT2017b model. However, as it stands, this particular test case does show the importance of evaluating the performance of these transition models over a large part of the multidimensional parameter space.

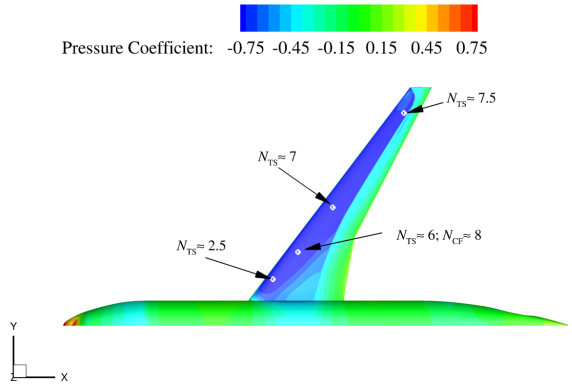

Fig. 16 Pressure distributions superimposed with TS and crossflow *N*-factors near selected locations along the transition front predicted via the LM2015 model on the suction side of the CRM wing for $Re_c = 15\times10^6$.

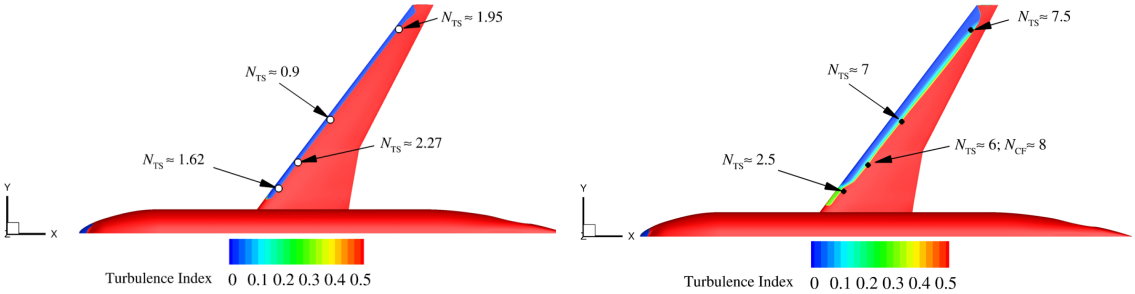

(a) AFT 2017b (b) LM2015

Fig. 17. Comparison of the predicted transition behavior on the suction surface of the wing shown using turbulence index contours for $Re_c = 15\times10^6$. Superimposed are TS and crossflow *N*-factors at the transition front computed using boundary layer stability analysis.

IV. Conclusions

An assessment of the current transition capabilities of the NASAs OVERFLOW CFD solver has been conducted, with a specific focus on swept-wing flow configurations with significant crossflow. Coder's AFT 2017b model and the Langtry-Menter transition model, both, without crossflow (LM2009) and with stationary crossflow effects (LM2015), were evaluated for a suite of test cases comprised of the NASA

NLF(2)-0415 45º swept-wing, the sickle-shaped wing by the Technical University of Braunschweig, and the wing-body configuration of the CRM model from the Fourth and Fifth AIAA CFD Drag Prediction workshops. The LM2015 model was best suited for all these cases, in that it was the only model that accounted (albeit indirectly) for the effects of both TS and CF instabilities. However, comparisons with linear stability characteristics of the CRM configuration indicate that, the AFT2017b model did not perform as well as the LM2009 and LM2015 models even when the CF effects are not particularly strong. This is probably because of an inadequate modeling of the stabilizing influence of flow compressibility on the TS amplification, given the heavy reliance of the AFT2017b model on correlations based on incompressible flows.

The present study has also highlighted the need to recalibrate the LM2015 model and describe our progress in that direction. A primary reason for this recalibration was related to the heavy reliance of correlations used in this model on the data from the NLF(2)-0415 45º swept-wing experiment and importance of correctly modeling the experimental setting in the CFD computations. A secondary reason was that the OVERFLOW implementation of the model was based on the latest, i.e., SST-2003 version of the RANS model, while the original formulation was based on the baseline version of the RANS model that has since been superseded by the SST-2003 version. The initial recalibration effort described in this paper did not account for the shift in the transition correlation for $(Re_{\theta t})_{SCF}$ as the strength of the boundary layer crossflow varies in relation to the reference configuration of the NLF(2)-0415 45º swept-wing experiment. However, while the recalibration was shown to yield a significant improvement in the transition predictions for the NLF(2)-0415 45º swept-wing, its impact was minimal for the sickle wing configuration. The recalibration effort did bring into focus the need to broaden the database, upon which the correlations for crossflow are derived, by acquiring data for other configurations for which the boundary layer transition process is dominated by stationary crossflow instability. These issues are being addressed in greater detail before these transition models and their OVERFLOW implementations, in particular, are used to model the CRM-NLF configuration in a parallel, ongoing effort. In turn, data from the CRM-NLF computations could also help to expand the basis for the calibration of these models.

Acknowledgments

This research is sponsored by the NASA Transformational Tools and Technologies (TTT) project of the Transformative Aeronautics Concepts Program under the Aeronautics Research Mission Directorate. The first two authors' research is funded through the National Institute of Aerospace (NIA) under the cooperative agreement 2A00 (Activity 201133).

References

[1] Slotnick, J., Khodahoust, A., Alonso, J., Darmofal, D., Gropp, W., and Mavriplis, D., "CFD Vision 2030 Study: A Path to Revolutionary Computational Aerosciences," NASA/CR-2014-218178, 2014.

[2] Smith, A. M. O., and Gamberoni, N., "Transition, Pressure Gradient and Stability Theory," Douglas Aircraft Company, Long Beach, Calif. Rep. ES 26338, 1956.

[3] van Ingen, J. L., "A suggested Semi-Empirical Method for the Calculation of the Boundary Layer Transition Region," University of Delft, Dept. of Aerospace Engineering, Delft, The Netherlands, Rep. VTH-74, 1956.

[4] Herbert, T., "Parabolized Stability Equations," *Annu. Rev. Fluid Mech.,* 29:245-283, 1997.

[5] Drela, M. and Giles, M. B., "Viscous-Inviscid Analysis of Transonic and Low Reynolds Number Airfoils," *AIAA Journal*, Vol. 25, No. 10, 1987, pp. 1347–1355.

[6] Drela, M., "Implicit Implementation of the Full e^N Transition Criterion," AIAA Paper 2003-4066, 2003.

[7] Cliquet, J., Houdeville, R., and Arnal, D., "Application of Laminar-Turbulent Transition Criterial in Navier-Stokes Computations," *AIAA Journal*, Vol. 46, No. 5, 2008, pp. 1182-1190.

[8] Perraud, J., Arnal, D., Casalis, G., Archambaud, J.-P., and Donelli, R., "Automatic Transition Predictions Using Simplified Methods," *AIAA Journal*, Vol.47, 2009, pp. 2676-2684.

[9] Krumbein, A., Krimmelbein, N., and Schrauf, G., "Automatic Transition Prediction in a Hybrid Flow Solver – Part 1: Methodology and Sensitivities," *J. Aircraft*, Vol. 46, No. 4, 2009, pp. 1176 – 1190.

[10] Krumbein, A., Krimmelbein, N., and Grabe, C., "Streamline-Based Transition Prediction Techniques in an Unstructured Computational Fluid Dynamics Code," *AIAA Journal*, Vol. 55, No. 5, 2017, pp. 1548–1564.

[11] Campbell, R., Campbell, M., and Streit, T., "Progress Toward Efficient Laminar Flow Analysis and Design," AIAA 2011-3527.
[12] Davis, M. B., Reed, H. L., Youngren, H., Smith, B., and Bender, E., "Transition Prediction Method Review Summary for the Rapid Assessment Tool for Transition Prediction (RATTraP)," Technical Report AFRL-VA-WP-TR-2005-3130, Air Force Research Lab, Wright-Patterson AFB, OH, 2005.
[13] Stock, H. W., and Haase, W., "Navier-Stokes Airfoil Computations with e^N Transition Prediction Including Transitional Flow Regions," *AIAA Journal,* Vol. 38, No. 11, 2000, pp. 2059–2066.
[14] Warren, E. S., and Hassan, H. A., "Transition Closure Model for Predicting Transition Onset," *J. Aircraft*, Vol. 35, No. 5, September–October 1998, pp. 769–775.
[15] Edwards, J. R., Roy, C. J., Blottner, F. G., and Hassan, H. A., "Development of a One-Equation Transition/Turbulence Model," *AIAA Journal*, Vol. 39, No. 9, 2001, pp. 1691–1698.
[16] Walters, D. K., and Leylek, J. H., "A New Model for Boundary-Layer Transition Using a Single-Point RANS Approach," *ASME J. of Turbomach*, Vol. 126(1), 2004, pp. 193–202.
[17] Menter, F. R., Langtry, R. B., and Völker, S., "Transition Modelling for General Purpose CFD Codes," *J. Flow, Turbulence and Combustion,* Vol.77, 2006, pp. 277–303.
[18] Langtry, R. B., and Menter, F. R., "Correlation-Based Transition Modeling for Unstructured Parallelized Computational Fluid Dynamics Codes," *AIAA Journal*, Vol. 47, 2009, pp. 2894–2906.
[19] Medida, S., and Baeder, J., "Application of the Correlation-based the γ-$\mathrm{Re}_{\theta t}$ Transition Model to the Spalart-Allmaras Turbulence Model," AIAA Paper 2011-3979, 2011.
[20] Ge, X., Arolla, S., and Durbin, P., "A Bypass Transition Model Based on the Intermittency Function," *J. Flow Turbulence and Combustion,* Vol.93, 2014, pp. 37–61.
[21] Song Fu, A., Wang, L., "RANS modeling of high-speed aerodynamic flow transition with consideration of stability theory," *Progress in Aerospace Sciences*, Vol. 58, 2013, pp. 36–59.
[22] Coder, J.G., and Maughmer, M.D., "Computational Fluid Dynamics Compatible Transition Modeling Using an Amplification Factor Transport Equation," *AIAA J*, Vol. 52, 2014, pp.2506–2512.
[23] Coder, J.G., "Further Development of the Amplification Factor Transport Transition Model for Aerodynamic Flows," AIAA Paper 2019-0039, 2019.
[24] Medida, S., "*Correlation-based Transition Modeling for External Aerodynamic Flows,*" University of Maryland Ph.D. Dissertation, 2014.
[25] Krumbein, A., Krimmelbein, N., Grabe, C. and Shengyang, N., "Development and Application of Transition Prediction Techniques in an Unstructured CFD Code," AIAA Paper 2015-2476, 2015.
[26] Nichols, R. H, and Buning, P. G., "User's Manual for OVERFLOW 2.2, Version 2.2," NASA Langley Research Center, Hampton, VA, Aug 2010.
[27] Lynde, M. N., Campbell, R. L., Rivers, M. B., Viken, S. A., Chan, D. T., Watkins, A. N., and Goodliff, S. L., "Preliminary Results from an Experimental Assessment of a Natural Laminar Flow Design Method," AIAA Paper 2019-2298, 2019.
[28] Rivers, M., Lynde, M., Campbell, R., Viken, S., Chan, D., Watkins, A., and Goodliff, S., "Experimental Investigation of the NASA Common Research Model with a Natural Laminar Flow Wing in the NASA Langley National Transonic Facility," AIAA Paper 2019-2189, 2019.
[29] Lynde, M. N., Campbell, R. L., and Viken, S. A., "Additional Findings from the Common Research Model Natural Laminar Flow Wind Tunnel Test," AIAA Paper 2019-2298, 2019.
[30] Medida, S., and Baeder, J., "A New Crossflow Transition Onset Criterion for RANS Turbulence Models," AIAA 2013-3081, 2013.
[31] Choi, J., and Kwon, O. J., "Enhancement of a Correlation-Based Transition Turbulence Model for Simulating Crossflow Instability," AIAA 2014-1133, 2014.
[32] Langtry, R. B., Sengupta, K., Yeh, D. T., and Dorgan, A. J., "Extending the γ-$\mathrm{Re}_{\theta t}$ Correlation based Transition Model for Crossflow Effects," AIAA Paper 2015-2474, 2015.
[33] Choi, J. H., and Kwon, O. J., "Recent Improvement of a Correlation-based Transition Model for Simulating Three-Dimensional Boundary Layers," *AIAA Journal*, Vol. 55, No. 6, 2017, pp. 2103–2108.
[34] Grabe, C., Shengyang, N., and Krumbein, A., "Transport Modeling for the Prediction of Crossflow Transition," *AIAA Journal,* Vol.56, 2018, pp.3167–3178.
[35] Nie, S., Krimmelbein, N., Krumbein, A., and Grabe, C., "Extension of a Reynolds-Stress-Based Transition Transport Model for Crossflow Transition," *J. Aircraft*, Vol. 55, 2018, pp. 1641–1654.
[36] Xu, J., Han, X., Qiao, L., Bai, J., and Zhang, Y., "Fully Local Amplification Factor Transport Equation for Stationary Crossflow Instabilities," *AIAA Journal*, Vol. 57, No. 7, 2019, pp. 2682–2693.
[37] Dagenhart, J. R., Saric, W. S., Mousseux, M. C., and Stack, J. P., "Crossflow-Vortex Instability and Transition on a 45-Degree Swept Wing," AIAA Paper 89-1892, 1989.
[38] Radeztsky, R., Reibert, M., and Saric, W., "Effect of Micron-Sized Roughness on Transition in Swept-Wing Flows," AIAA Paper 93-0076, 1993.
[39] Dagenhart, J. R., and Saric, W. S., "Crossflow Stability and Transition in Swept Wing Flow," NASA TP-1999-209344, 1999.

[40] Petzold, R. and Radespiel, R., "Transition on a Wing with Spanwise Varying Crossflow and Linear Stability Analysis," *AIAA Journal*, Vol. 53, No. 2, 2015, pp. 321-325.
[41] Vassberg, J.C., DeHaan, M.A., Rivers, M.S., and Wahls, R.A., "Retrospective on the Common Research Model for Computational Fluid Dynamics Validation Studies," *J. Aircraft*, Vol. 55, 2018, pp. 1325–1337.
[42] Menter, F. R., Kuntz, M., and Langtry, R., "Ten Years of Industrial Experience with the SST Turbulence Model," Turbulence, Heat and Mass Transfer 4, ed: K. Hanjalic, Y. Nagano, and M. Tummers, Begell House, Inc., 2003, pp. 625–632.
[43] Spalart, P. R. and Allmaras, S. R., "A One-Equation Turbulence Model for Aerodynamic Flows," Recherche Aerospatiale, No. 1, 1994, pp. 5-21.
[44] Menter, F. R., "Two-Equation Eddy-Viscosity Turbulence Models for Engineering Applications," *AIAA Journal*, Vol. 32, No. 8, August 1994, pp. 1598-1605.
[45] Roe, P. L., "Approximate Riemann Solvers, Parameter Vectors, and Difference Schemes," *J. Comput Phys.,* Vol. 43, No. 2, 1981, pp. 357–372.
[46] Nichols, R. H., Tramel, R. W., and Buning, P. G., "Solver and Turbulence Model Upgrades to OVERFLOW 2 for Unsteady and High-Speed Applications," AIAA Paper 2006-2824, 2006.
[47] Somers, D. M., and Horstmann, K. H., "Design of a Medium Speed Natural-Laminar Flow Airfoil for Commuter Aircraft Applications," DFVLR-IB.29-85/26, 1985.
[48] Crouch, J. D., and Ng, L. L., "Variable N-Factor Method for Transition Prediction in Three-Dimensional Boundary Layers," *AIAA Journal*, Vol. 38, No. 2, 2000, pp. 211–216.
[49] Chan, W. M., "CAD Interface, Strand Grid Technology, and Other New Developments in Chimera Grid Tools 2.0," Proceedings of the 8th Symposium on Overset Composite Grids and Solution Technology, Houston, Texas, October, 2006.
[50] Suhs, N. E., Rogers, S. E., and Dietz, W. E., "PEGASUS 5: An Automatic Pre-Processor for Overset-Grid CFD," AIAA Paper 2002-3186, 2002.
[51] Wie, Y., "BLSTA – A Boundary Layer Code for Stability Analysis," NASA CR-4481, 1992.
[52] Chang, C.-L., "The Langley Stability and Transition Analysis Codes (LASTRAC): LST, Linear & Nonlinear PSE for 2D, Axisymmetric and Infinite Swept Wing Boundary Layers," AIAA paper 2003-0974, 2003.
[53] Sclafani, A., Slotnick, J., Vassberg, J. and Pulliam, T., "Extended OVERFLOW Analysis of the NASA Trap Wing Wind Tunnel Model," AIAA Paper 2012-2919, 2012.
[54] Coder, J., "Standard Test Cases for CFD-Based Laminar-Transition Model Verification and Validation," AIAA Paper 2018-0029, 2018.
[55] Biedron, R. T., Carlson, J.-R., Derlaga, J. M., Gnoffo, P. A., Hammond, D. P., Jones, W. T., Kleb, B., Lee-Rausch, E. M., Nielsen, E. J., Park, M. A., Rumsey, C. L., Thomas, J. L., and Wood, W. A., "FUN3D Manual: 12.9," NASA-TM-2016-219012, 2016
[56] Vassberg, J. C., "Unified Baseline Grid About the Common Research Model Wing-Body for the Fifth AIAA CFD Drag Prediction Workshop," AIAA Paper 2011-3508, 2011.
[57] Crouch, J., Sutanto, M., Witkowski, D., Watkins, A., Rivers, M., and Campbell, R., "Assessment of the National Transonic Facility for Natural Laminar Flow Testing," AIAA Paper 2010-1302, 2010.